JOC The Journal of Organic Chemistry

Article

pubs.acs.org/joc

Origins of Regioselectivity in the Fischer Indole Synthesis of a Selective Androgen Receptor Modulator

Elizabeth L. Noey,[†] Zhongyue Yang,[†] Yanwei Li,[†] Hannah Yu,[‡] Rachel N. Richey,[‡] Jeremy M. Merritt,[‡] Douglas P. Kjell,[‡] and K. N. Houk*[,†]

[†]Department of Chemistry and Biochemistry, University of California, Los Angeles, California 90095, United States

[‡]Eli Lilly and Co., Lilly Corporate Center, Indianapolis, Indiana 46285, United States

Supporting Information

ABSTRACT: The selective androgen receptor modulator, (*S*)-(7-cyano-4-(pyridin-2-ylmethyl)-1,2,3,4-tetrahydrocyclopenta-[*b*]indol-2-yl)carbamic acid isopropyl ester, LY2452473, is a promising treatment of side effects of prostate cancer therapies. An acid-catalyzed Fischer indolization is a central step in its synthesis. The reaction leads to only one of the two possible indole regioisomers, along with minor decomposition products. Computations show that the formation of the observed indole is most favored energetically, while the potential pathway to the minor isomer leads instead to decomposition products. The disfavored [3,3]-sigmatropic rearrangement, which would produce the unobserved indole product, is destabilized by the electron-withdrawing phthalimide substituent. The most favored [3,3]-sigmatropic rearrangement transition state is bimodal, leading to two reaction intermediates from one transition state, which is confirmed by molecular dynamics simulations. Both intermediates can lead to the observed indole product, albeit through different mechanisms.

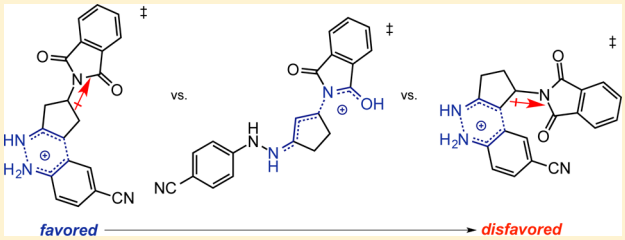

INTRODUCTION

Indole derivatives have extensive biological activity and are important in pharmaceuticals.[1,2] The venerable Fischer indole synthesis[3] continues to be a widely applicable approaches to the synthesis of indoles.

Indole **1**,[4] named LY2452473 (Figure 1), is a selective androgen receptor modulator (SARM), and has been brought to phase 1 clinical trials for the treatment of secondary hypogonadism induced by androgen deprivation therapy (ADT). ADT reduces the levels of androgens, or male hormones, which stimulate prostate cancer cells. However, ADT has a variety of side effects,[5] which indole **1** shows promise in combatting.

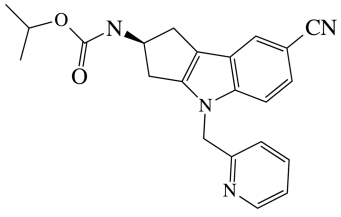

1

Figure 1. Indole **1**, LY2452473, a SARM, is a clinical candidate to treat symptoms of androgen deprivation therapy.[4]

Çelebi-Ölçüm et al.[6] showed that in the acid-catalyzed Fischer indole synthesis either the arene or enamine nitrogen, Nα or Nβ, respectively, can be protonated to accelerate the [3,3]-sigmatropic rearrangement (Figure 2). Protonation of Nβ is favored and leads to the lowest energy rearrangement.

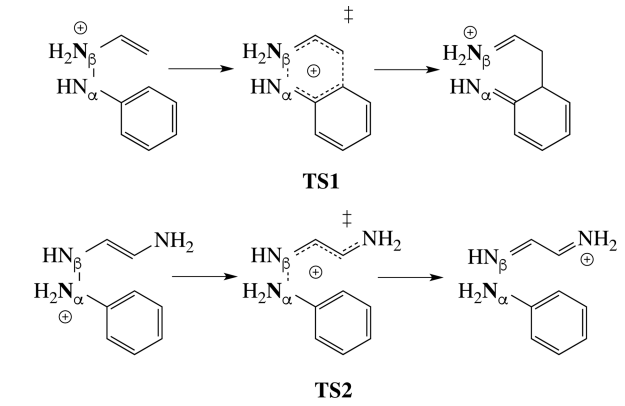

Figure 2. [3,3]-Sigmatropic rearrangement in the Fischer indolization.

Protonation of Nα is disfavored by 1.5 kcal/mol, and the thermal reaction of this species is disfavored by 12.6 kcal/mol.

In the current study, as shown in Figure 3, the hydrazine **2** reacts with the cyclopentanone **3** under acidic conditions to form only one indole regioisomeric product, **4**. A variety of reaction conditions were screened, resulting in differing yields

Received: April 12, 2017
Published: May 3, 2017

DOI: 10.1021/acs.joc.7b00878
J. Org. Chem. 2017, 82, 5904−5909

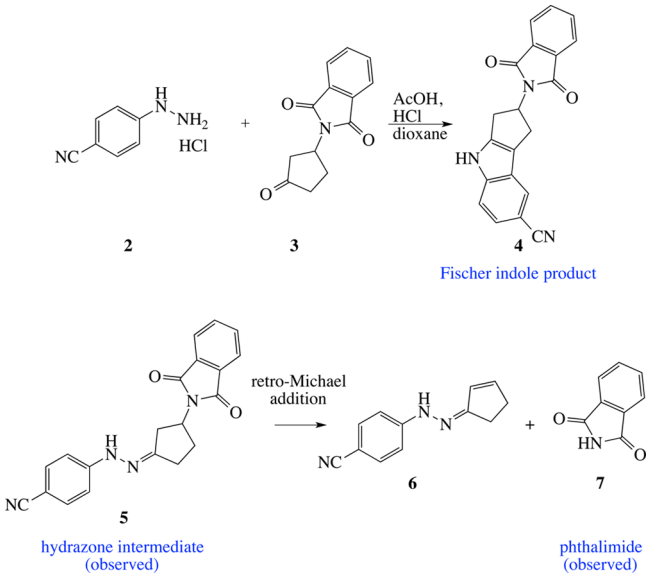

Figure 3. Experimental Fischer indolization and observed side products.

and side products **5** and **7**, among other uncharacterized side products. The isolation of hydrazone **5** indicates the reaction does not go to completion under certain conditions, and the isolation of phthalimide **7** suggests the decomposition reaction shown. No cyclopentenone is observed, indicating that **7** is not the result of the decomposition of starting material **3**. In all cases, the isomeric indole, **8**, is not formed (Figure 4).

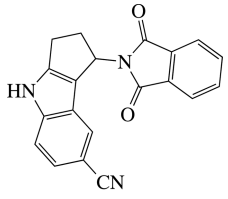

Figure 4. Unobserved indole regioisomer.

RESULTS AND DISCUSSION

Figure 5 shows the reaction pathways explored computationally. The hydrazone intermediate **5** can form two indole regioisomers **4** and **8** as well as decomposition products **6** and **7**. Free energies of each intermediate and several relevant transition states are shown. The hydrazone intermediate **5** is preferentially protonated at Nβ. This will be in equilibrium with the hydrazone protonated at Nα or at the phthalimide O. Either of the two carbons β to the hydrazone N on the cyclohexane ring (i.e., C2 or C5) can be deprotonated to form two regioisomeric enamine intermediates, which can also be protonated at Nα, Nβ, or O and are in equilibrium with the hydrazone. For the formation of the observed indole product, **4**, the deprotonation occurs at C5 and forms enamine **9**. Enamine **9-Nα** undergoes the [3,3]-sigmatropic rearrangement via **TS2-Nα***, which has an energy of 33.4 kcal/mol relative to hydrazone **5-Nβ**. This forms **10-Nα** or **13-Nα**, which eventually lead to the observed indole product, **4**.

The enamine formed from deprotonation at C2, **11**, decomposes by a retro-Michael reaction through **TS4-O** to form **6** and **7**. Decomposition of **11** is favored over the [3,3]-sigmatropic rearrangement via **TS3-Nβ** by 1.8 kcal/mol. This explains why the indole regioisomer **8** is not observed. Decomposition of enamine **11** is disfavored by 1.8 kcal/mol compared to the formation of the observed indole **4** by the amount discussed above.

Figure 6 shows the most favored transition structure for [3,3]-sigmatropic rearrangement, **TS2-Nα***, which is on a bifurcating potential surface and leads to two products. Because the intermediates share a common transition structure, dynamics control the product distribution.[7] This bifurcation happens when Nα is protonated, and the phthalimide is oriented with one O near the reacting moieties. This is because the arene carbon and the phthalimide oxygen are competing nucleophiles toward the enamine motif. The competing nucleophiles stabilize the partially positively charged β-carbon. On the bifurcating surface, the first transition state, **TS2-Nα***, involves primarily breaking of the N−N bond, while the second, a transition state for the interconversion of the products, either forms the C−C or C−O bond. The formation of the C−C bond gives the rearrangement product, **10-Nα**, and the formation of the C−O bond gives a [3.2.1] bridged heterocycle, **13-Nα**.

Reaction dynamics simulations were performed to investigate the bifurcation of the [3,3]-sigmatropic rearrangement of enamine **9-Nα**. Normal mode sampling was conducted on the **TS2-Nα*** to obtain an ensemble of TS geometries, as shown in Figure 7. The formation of bonds 2 and 4 leads to **10-Nα** and **13-Nα**, respectively. The distributions of bond lengths for these two bonds are identical, which suggests that **10-Nα** and **13-Nα** should have equal chance of formation. The formation of bond 3, on the other hand, also results in **10-Nα**, through a chair−Cope-like pathway. Bond 3 is 0.4 Å longer than bond 2 or 4 in the transition structure, leaving the question of whether **10-Nα** is also produced by the formation of bond 3. This bond has a distribution of 3.50 ± 0.38 Å, which partially overlaps with that of bond 2.

One hundred and eighty trajectories were initiated from the TS geometries. Trajectories were propagated forward and backward until the formation of the product **10-Nα** (bond 1 >3.5 Å and bond 2 < 1.5 Å, or bond 3 <1.5 Å), or **13-Nα** (bond 1 >3.5 Å and bond 4 <1.5 Å), or the formation of the reactant **9-Nα** (bond 1 <1.5 Å, bond 2 >3.5 Å, and bond 4 >3.5 Å). Trajectories were terminated after 500 fs if neither criteria was met. Both **10-Nα** and **13-Nα** were observed in the simulation. One hundred and sixty trajectories were productive, and 20 were recrossing. Among these reactive trajectories, 79 (49.3%) gave **10-Nα** by forming bond 2 and one (0.7%) by bond 3, 78 (48.7%) formed **13-Nα**, and two (1.3%) bridged **10-Nα** and **13-Nα**. The trajectories bridging **10-Nα** and **13-Nα** were observed because the sampled transition-state geometries slightly overlap the transition state **TS7-Nα**. Figure 8 shows the distribution of 10 representative trajectories leading to **10-Nα** and **13-Nα** and typical snapshots for the formation of these two products. The transition zone is labeled in red, which was previously defined as the region that embraces 98% of the transition-state geometries. As bond 1 (N−N bond) elongates, trajectories pass the transition zone and start to bifurcate when bond 1 is ∼3.0 Å.

Figure 9 shows how the products of the bifurcation lead to the observed product through different routes. The separate molecules of **13-Nα** likely do not completely react with each other. From intermediate **13-Nα** there is a low barrier (23.7

DOI: 10.1021/acs.joc.7b00878
J. Org. Chem. 2017, 82, 5904−5909

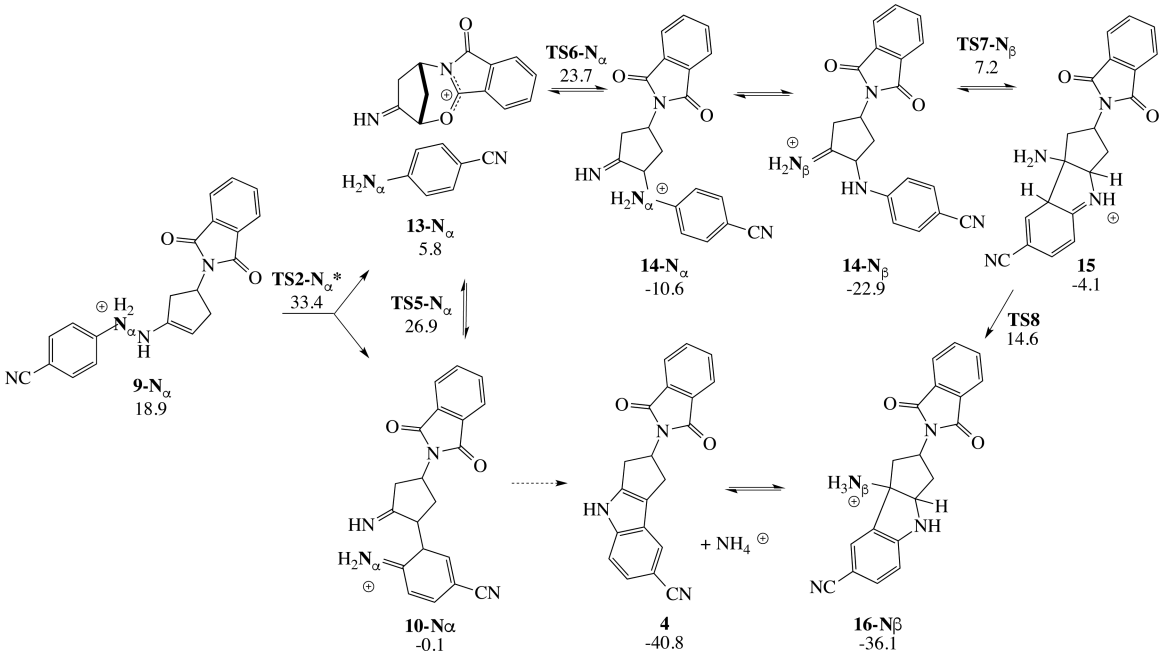

Figure 5. Competing pathways from hydrazone **5-N*β*** to the two possible regioisomeric indoles **4** and **8** and decomposition products **6** and **7**. Δ*G* is given in kcal/mol.

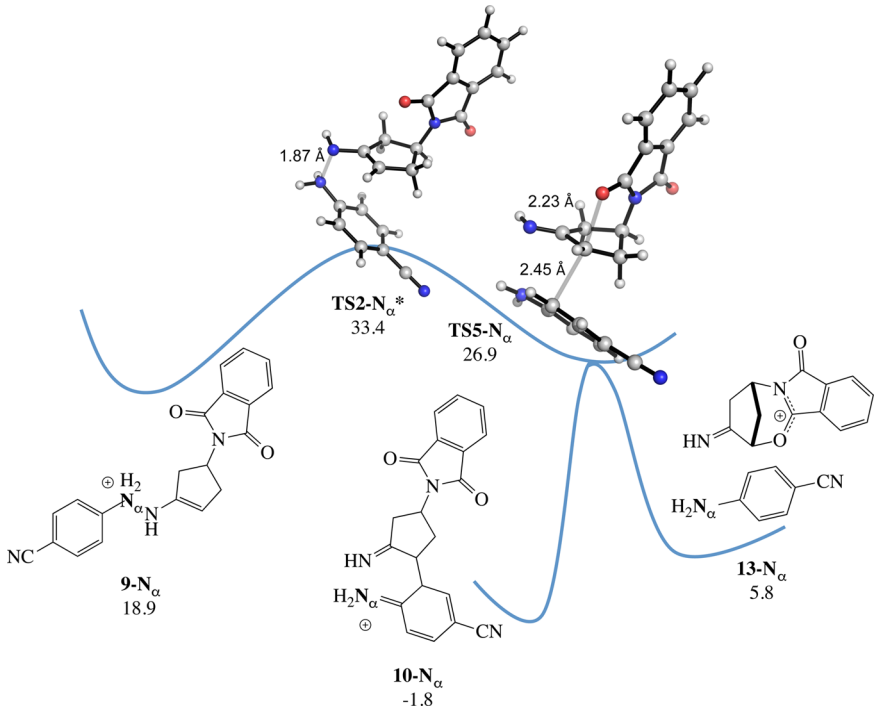

Figure 6. Bifurcating energy surface from **9-N*α***. Δ*G* is given in kcal/mol. Bond lengths are given in angstroms.

kcal/mol, **TS7-N*α***) for the attack of the cyanoaniline to form **14-N*α***. The transition structure for the competing deprotonation of **13-N*α*** to form the enimine (not shown) is 32.7 kcal/mol, 8.9 kcal/mol higher in energy than **TS7-N*α***. Intermediate **14-N*α*** can undergo proton transfer, followed by intramolecular attack of the arene on the imine to form **15**. This is followed by sequential deprotonation and loss of NH_4 to form the product.

The [3,3]-sigmatropic rearrangement transition state has many degrees of freedom: N*α* or N*β* may be positively charged, it can adopt a chair or boat conformation, and the arene can form a bond on the same or opposite side of the phthalimide. When the transition state is in a boat conformation the arene is over the cyclohexane ring, and it is not sterically possible for the phthalimide to be on the same side in this conformation. This means there were six conformations to explore. Additionally, the cyclohexane ring may adopt one of two envelope conformations, and only the lowest energy conformation is reported here. These transition states are reported in Table 1. There are two transition structures for the [3,3]-sigmatropic rearrangement for the observed regioisomer that are com-

DOI: 10.1021/acs.joc.7b00878
J. Org. Chem. 2017, 82, 5904−5909

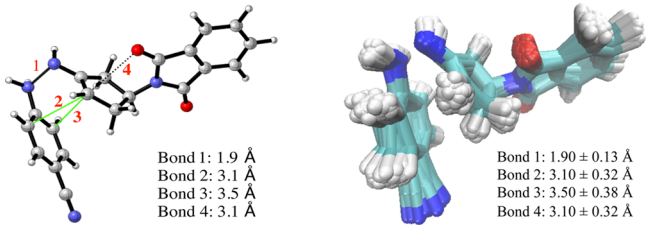

Figure 7. Structure of **TS2-Nα*** and the overlay of TS geometries obtained from normal model sampling.

parable in energy. The second one, only 0.4 kcal/mol higher in energy, is not bimodal and only leads to **10-Nα**. The energy of this transition structure is shown in Table 1 highlighted in bold text. It is in a chair conformation with Nα protonated, and the phthalimide on the same side as the arene.

The phthalimide group is electron-withdrawing, which has a greater destabilizing effect the closer it is to the positively charged reactive moiety. In the [3,3]-sigmatropic rearrangement for the formation of the observed regioisomer (**TS2**) the phthalimide is two carbons from the atoms involved in the rearrangement. In the formation of the unobserved regioisomer (**TS3**) it is only one carbon away. Therefore, the phthalimide destabilizes **TS3** more so than **TS2**, as indicated qualitatively in Figure 10.

The analogous [3,3]-sigmatropic rearrangement transition states en route to **8** are not bimodal. This is because the attack of the phthalimide oxygen on the enamine would form a strained 5-membered heterocycle. In the [3,3] transition state, the oxygen of the phthalimide is far from the β-C.

CONCLUSION

Our calculations explain the formation of only one regioisomeric indole product in the Fischer indolization used for the synthesis of **1** and account for the presence of decomposition product **6**. In the pathway to the observed indole product **4**, several [3,3]-sigmatropic rearrangement transition states are possible. The lowest energy path (**TS2-Nα***) is favored by 1.8 kcal/mol compared to the competing decomposition pathway through **TS4-O** and 3.6 kcal/mol compared to the formation of the unobserved indole **8** via **TS3-Nα**. The [3,3]-sigmatropic rearrangements from enamine **9**, **TS2-Nα**, experience less destabilization than the disfavored **TS3-Nα** because the atoms involved in the rearrangement are further from the phthalimide. The favored [3,3]-sigmatropic rearrangement, **TS2-Nα***, is bimodal, leading to two products from one transition state. Of the molecular dynamics simulations from **TS2-Nα*** 50.0% form **10-Nα**, 48.7% form **13-Nα**, and 1.3% bridge **10-Nα** and **13-Nα**. The two intermediates lead to the observed indole product by different paths. This work elucidates the driving force for the observed regioselectivity of this significant reaction. These calculations enable design of novel regioselective Fischer indolization reactions.

EXPERIMENTAL SECTION

All calculations were performed with Gaussian09.[8] Structures were optimized with M06-2X/6-31G(d) in the gas phase. Truhlar's quasiharmonic approximation was used to correct for errors in the estimation of vibrational entropies by setting all positive frequencies below 100 cm^{-1} to 100 cm^{-1}.[9] Single-point energy calculations used M06-2X/6-311+G(2d,p)[10] with the SMD solvation model[11] for acetic acid. Relative Gibb's free energies are reported in kcal/mol.

Direct molecular dynamics simulations were performed in the gas phase. Because of the demanding quantum calculations required in the dynamics simulations, these were performed at the M06-2X/6-31G(d) level of theory. Quasiclassical trajectories were initialized in the region of the potential energy surface near the transition state.[12] Normal-mode sampling involves adding zero-point energy for each real normal mode in the TS and then Boltzmann sampling to afford a set of geometries reflecting the thermal energy available at 300 K with a random phase.[13] No additional velocities were added other than vibrations along the mode perpendicular to the reaction coordinate. The trajectories were propagated forward and backward until the formation of product, or the reactant. The classical equations of motion were integrated with a velocity−Verlet algorithm using Singleton's program Progdyn,[14] with the energies and derivatives computed on the fly by the M06-2X method using Gaussian 09. The step length for integration was 1 fs.

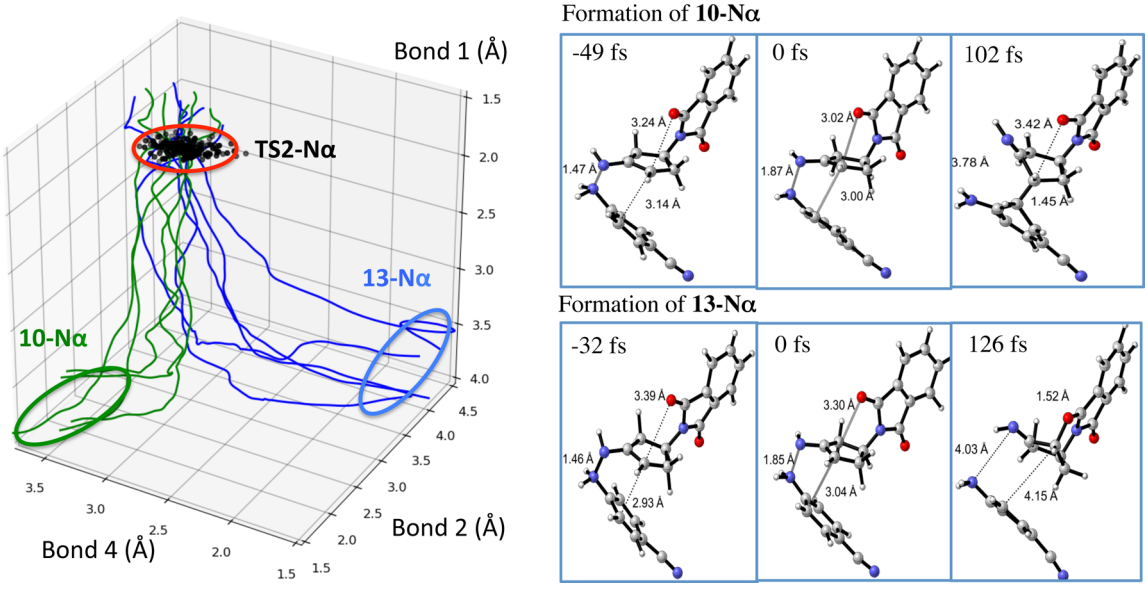

Figure 8. Distribution of ten representative trajectories and snapshots for the formation of **10-Nα** and **13-Nα**. The black dots represent the sampled transition-state geometries, and the red circle represents the transition zone.

DOI: 10.1021/acs.joc.7b00878
J. Org. Chem. 2017, 82, 5904−5909

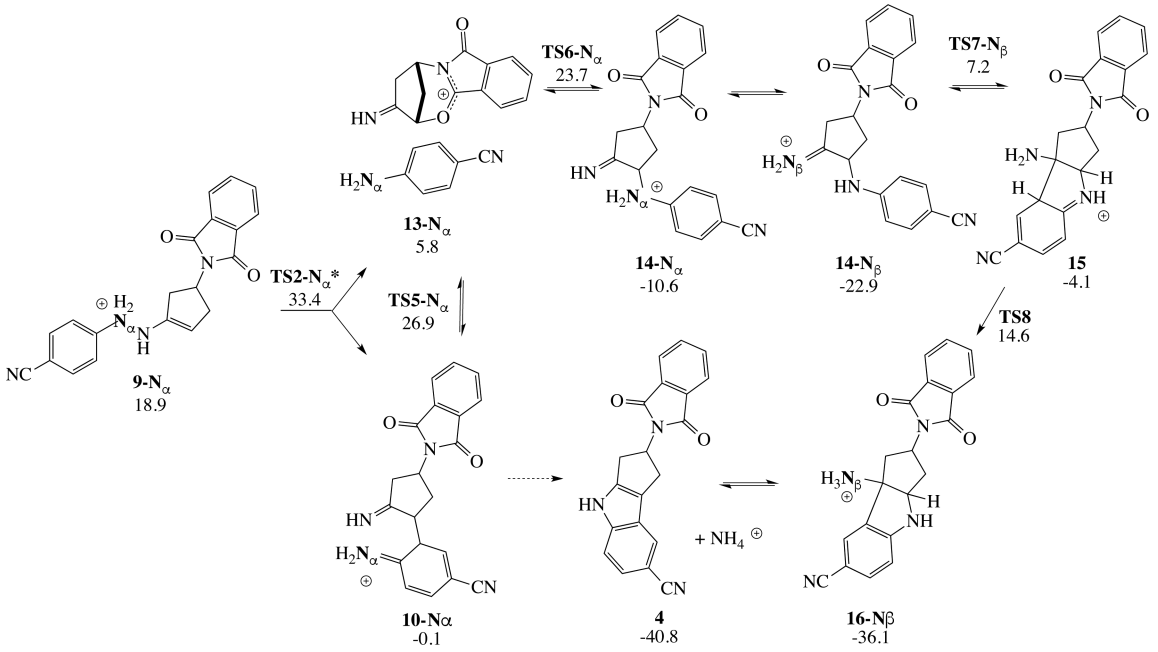

Figure 9. Competing pathways from **9-Nα**, including the bifurcation and competing paths to the observed indole product **4**. Δ*G* is given in kcal/mol.

Table 1. Δ*G* for the [3,3]-Sigmatropic Rearrangement Transition States[a]

	observed regioisomer				unobserved regioisomer			
	chair		boat		chair		boat	
relationship to phthalamide	Nα	Nβ	Nα	Nβ	Nα	Nβ	Nα	Nβ
same side	**34.4**	38.5	NA	NA	41.4	43.3	NA	NA
opposite side	36.2[b]	38.5	34.4	39.0	39.8	40.9	**38.6**	42.1

[a]"Chair" and "boat" indicate the conformation of the atoms involved in the [3,3]-sigmatropic rearrangement, and Nα and Nβ refer to where the positive charge resides. The energy of the lowest energy transition structures for the observed and unobserved regioisomers, **TS2-Nα** and **TS3-Nα**, respectively, are shown in boldface and also reported in Figure 5. [b]bimodal.

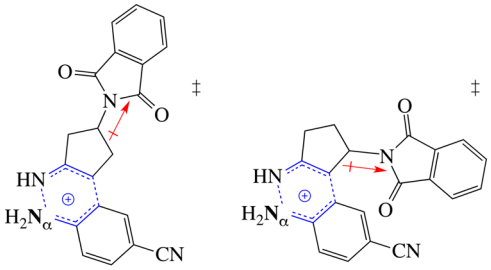

Figure 10. Transition states for the [3,3]-sigmatropic rearrangement. The phthalimide is further from the positive charge in the favored transition state (**TS2**) than it is in disfavored transition state (**TS3**).

■ ASSOCIATED CONTENT

Supporting Information

The Supporting Information is available free of charge on the ACS Publications website at DOI: 10.1021/acs.joc.7b00878.

High-throughput liquid chromatography trace from the Fischer indolization reaction, absolute energies, imaginary frequencies, and Cartesian coordinates for all structures, energies, and bond lengths of transition states and intermediates involved in the bifurcating surfaces (PDF)

■ AUTHOR INFORMATION

Corresponding Author

*E-mail: houk@chem.ucla.edu.

ORCID

Elizabeth L. Noey: 0000-0001-9067-0443

K. N. Houk: 0000-0002-8387-5261

Notes

The authors declare no competing financial interest.

■ ACKNOWLEDGMENTS

We are grateful to the National Science Foundation (CHE-1361104) for financial support of this research. Calculations were performed on the Hoffman2 cluster at UCLA and the Extreme Science and Engineering Discovery Environment (XSEDE), which is supported by the NSF (OCI-1053575). We thank Natalie C. James and Hao Wang for preliminary computational results.

■ REFERENCES

(1) *Indole Ring Synthesis — From Natural Products to Drug Discovery*; Gribble, G.W., Ed.; Wiley, 2016.

DOI: 10.1021/acs.joc.7b00878
J. Org. Chem. 2017, 82, 5904−5909

(2) Humphrey, G. R.; Kuethe, J. T. *Chem. Rev.* **2006**, *106*, 2875−2911.
(3) (a) Fischer, E.; Jourdan, F. *Ber. Dtsch. Chem. Ges.* **1883**, *16*, 2241−2245. (b) Fischer, E.; Hess, O. *Ber. Dtsch. Chem. Ges.* **1884**, *17*, 559−568.
(4) (a) Fales, K. R.; Green, J. E.; Jadhav, P. K.; Matthews, D. P.; Neel, D. A.; Smith, E. C. R.; Tetrahydrocarbazole derivatives useful as androgen receptor modulators, WO2007002181A2, Jan 4, 2007. (b) Jadhav, P. K.; Krishnan, V.; Kim, E. J., Tetrahydrocyclopenta[b]-indole androgen receptor modulators. WO2009140448A1, Nov 19, 2009. (c) Benson, C. T., Treatment of Androgen Deprivation Therapy Associated Symptoms. WO 2016040234Al, Sep 8, 2015.
(5) (a) Nguyen, P. L.; Alibhai, S. M.; Basaria, S.; D'Amico, A. V.; Kantoff, P. W.; Keating, N. L.; Penson, D. F.; Rosario, D. J.; Tombal, B.; Smith, M. R. *Eur. Urol.* **2015**, *67*, 825−836. (b) Krupski, T. L.; Smith, M. R.; Chan Lee, W.; Pashos, C. L.; Brandman, J.; Wang, Q.; Botteman, M.; Litwin, M. S. *Cancer* **2004**, *101*, 541−549. (c) Wilke, D. R.; Parker, C.; Andonowski, A.; Tsuji, D.; Catton, C.; Gospodarowicz, M.; Warde, P. *BJU Int.* **2006**, *97*, 963−968.
(6) Çelebi-Ölçüm, N.; Boal, B. W.; Huters, A. D.; Garg, N. K.; Houk, K. N. *J. Am. Chem. Soc.* **2011**, *133*, 5752−5755.
(7) (a) Ess, D. H.; Wheeler, S. E.; Iafe, R. G.; Xu, L.; Çelebi- Ölçüm, N.; Houk, K. N. *Angew. Chem., Int. Ed.* **2008**, *47*, 7592−7601. (b) Thomas, J. B.; Waas, J. R.; Harmata, M.; Singleton, D. *J. Am. Chem. Soc.* **2008**, *130*, 14544−14555. (c) Martin-Somer, A.; Yanez, M.; Hase, W. L.; Gaigeot, M.-P.; Spezia, R. *J. Chem. Theory Comput.* **2016**, *12*, 974−982.
(8) *Gaussian 09*, revision D.01: Frisch, M. J.; Trucks, G. W.; Schlegel, H. B.; Scuseria, G. E.; Robb, M. A.; Cheeseman, J. R.; Scalmani, G.; Barone, V.; Mennucci, B.; Petersson, G. A.; Nakatsuji, H.; Caricato, M.; Li, X.; Hratchian, H. P.; Izmaylov, A. F.; Bloino, J.; Zheng, G.; Sonneerg, J. L.; Hada, M.; Ehara, M.; Toyota, K.; Fukuda, R.; Hasegawa, J.; Ishida, M.; Nakajima, T.; Honda, Y.; Kitao, O.; Nakai, H.; Vreven, T.; Montgomery, J. A., Jr.; Peralta, J. E.; Ogliaro, F.; Bearpark, M.; Heyd, J. J.; Brothers, E.; Kudin, K. N.; Staroverov, V. N.; Kobayashi, R.; Normand, J.; Raghavachari, K.; Rendell, A.; Burant, J. C.; Iyengar, S. S.; Tomasi, J.; Cossi, M.; Rega, N.; Millam, M. J.; Klene, M.; Knox, J. E.; Cross, J. B.; Bakken, V.; Adamo, C.; Jaramillo, J.; Gomperts, R.; Stratmann, R. E.; Yazyev, O.; Austin, A. J.; Cammi, R.; Pomelli, C.; Ochterski, J. W.; Martin, R. L.; Morokuma, K.; Zakrzewski, V. G.; Voth, G. A.; Salvador, P.; Dannenberg, J. J.; Dapprich, S.; Daniels, A. D.; Farkas, Ö.; Foresman, J. B.; Ortiz, J. V.; Cioslowski, J.; Fox, D. J. Gaussian, Inc., Wallingford, CT, 2009.
(9) Ribeiro, R. F.; Marenich, A. V.; Cramer, C. J.; Truhlar, D. G. *J. Phys. Chem. B* **2011**, *115*, 14556−14562.
(10) (a) Zhao, Y.; Truhlar, D. G. *Theor. Chem. Acc.* **2008**, *120*, 215−241. (b) Zhao, Y.; Truhlar, D. G. *Acc. Chem. Res.* **2008**, *41*, 157−167.
(11) Marenich, A. V.; Cramer, C. J.; Truhlar, D. G. *J. Phys. Chem. B* **2009**, *113*, 6378−6396.
(12) (a) Yang, Z.; Doubleday, C.; Houk, K. N. *J. Chem. Theory Comput.* **2015**, *11*, 5606−5612. (b) Yang, Z.; Yu, P.; Houk, K. N. *J. Am. Chem. Soc.* **2016**, *138*, 4237−4242.
(13) (a) Doubleday, C.; Bolton, K.; Hase, W. L. *J. Phys. Chem. A* **1998**, *102*, 3648−3658. (b) Black, K.; Liu, P.; Xu, L.; Doubleday, C.; Houk, K. N. *Proc. Natl. Acad. Sci. U. S. A.* **2012**, *109*, 12860−12865. (c) Bunker, D. L.; Hase, W. L. *J. Chem. Phys.* **1973**, *59*, 4621−4632.
(14) Oyola, Y.; Singleton, D. A. *J. Am. Chem. Soc.* **2009**, *131*, 3130−3131.

DOI: 10.1021/acs.joc.7b00878
J. Org. Chem. 2017, 82, 5904−5909